Construction and Building Materials 369 (2023) 130615

Contents lists available at ScienceDirect

Construction and Building Materials

journal homepage: www.elsevier.com/locate/conbuildmat

Three-dimensional FEM–DEM coupling simulation for analysis of asphalt mixture responses under rolling tire loads

Haitao Ge [a,*], Juan Carlos Quezada [a], Vincent Le Houerou [b], Cyrille Chazallon [a]

[a] Université de Strasbourg, INSA de Strasbourg, CNRS, ICube, UMR 7357, F-67000 Strasbourg, France
[b] Université de Strasbourg, CNRS, ICube, UMR 7357, F-67000 Strasbourg, France

ARTICLE INFO

Keywords:
Asphalt mixture
Finite Element Method
Discrete Element Method
FEM–DEM coupling
Rolling tire
Tire–pavement interaction

ABSTRACT

As traffic grows by leaps and bounds, deterioration of asphalt surface layers emerges as the primary cause of road network costs. A deep understanding of the tire–pavement interaction is essential for optimizing the surface design of asphalt pavements in the context of aging infrastructure and limited maintenance resources. Most of the current tire–pavement interaction studies have been conducted in the continuum mechanics framework using Finite Element Methods (FEM), which shows limitations in modeling the discontinuity nature of asphalt mixtures. Discrete Element Methods (DEM) offer a promising way to examine the mechanical properties of asphalt mixtures at the particle level, but it is inadequate for modeling deformable tire structure and capturing realistic tire contact forces on the pavement surface. In this study, a FEM–DEM coupling strategy was developed for the modeling of tire–pavement interaction by implementing a DEM model of asphalt mixtures with rolling tire loads from a FEM model. Based on simulations with realistic rolling tire load conditions, this coupling algorithm allows the investigation of particle force chain network evolution, particle displacement and velocity distributions, movements of individual particles, and particle contact force characteristics inside an asphalt mixture. This study offers an enriching expansion of both continuum and discrete mechanics methods for analyzing asphalt mixture responses under rolling tire loads, which can provide insight into pavement surface design.

1. Introduction

1.1. Motivation

Asphalt mixtures are complex multi-phase composite materials extensively used in road construction, such as highways and urban pavements. A significant part of road network costs is related to surface degradation, which tends to occur most frequently on asphalt surface layers. Due to its heterogeneous structure, the material response of an asphalt mixture is determined by properties of its components (aggregates, asphalt binder, and air voids), changing environmental variables (temperature, moisture, etc.) and interaction with loading tires. Therefore, it is crucial to assess the mixture responses at a micro-structural level under real tire load conditions in order to better understand and model its behavior.

Asphalt mixtures under rolling tire loads are subjected to three-dimensional stress states with varying stress levels in each dimension. Therefore, it is usually difficult to achieve such complex boundary conditions through laboratory tests due to the limited capabilities of testing equipment and measurement systems. Full-scale tests based on the Accelerated Pavement Testing (APT) method [1–4] are an effective approach for assessing macroscopic pavement performance under real tire loading. However, it is still a struggle to get insight into the internal mechanisms of the mixture damage at a microscopic point of view by using APT.

To cope the difficulties rising from the complexity and inadequacy of experimental measurements, numerical approaches such as the Finite Element Method (FEM) and the Discrete Element Method (DEM) have emerged as a promising and effective way of gaining insight into asphalt mixture performance in recent decades.

For simulating a dynamic mutual interaction system comprising a tire and an asphalt mixture at the micro-structural level, three issues need to be addressed primarily: Firstly, seeking a realistic representation for the tire load; Secondly, modeling an asphalt mixture while explicitly considering characteristics of its different components (irregular aggregate particles, asphalt binder, etc.); Finally, applying the rolling tire load to the mixture structure by coupling the two models above. In the following, we discuss the tire modeling and modeling of microscopic asphalt mixtures to solve the first two problems. For the

* Corresponding author.
E-mail address: haitao.ge@etu.unistra.fr (H. Ge).

https://doi.org/10.1016/j.conbuildmat.2023.130615
Received 21 June 2022; Received in revised form 29 September 2022; Accepted 31 January 2023

final issue, a coupling strategy is introduced to address the simulation of asphalt mixture responses at the particle level under rolling tire loads.

1.2. Literature review of tire modeling

As a prerequisite to investigating asphalt pavement performance under tire loads, it is essential to represent tire contact stresses on the pavement surface realistically. Currently, tire load distributions can either be obtained from measurements [5–7] or from numerical models. Due to the limitations of experimental measurements in studying different boundary conditions, experimental approaches struggle to examine this interaction system adequately. On the other hand, numerical tools provide an effective way to explore this system, especially, the FEM is widely used in the tire modeling investigation. Several FEM tire models were built to study tire contact stresses under different working conditions, such as the models developed by Korunović et al. [8], Wang et al. [9], Wollny et al. [10,11], and Guo et al. [12,13]. The results showed that tire contact stresses are influenced by multiple factors, including tire structure, inflation pressure, tire load, rolling states (free rolling, acceleration/braking, and cornering), rolling speed, friction, etc.

However, in the most current research, the pavement structure was assumed as rigid in the tire–pavement model, and the contact stresses on the tire were calculated to reflect tire load distribution on the pavement surface. Although this assumption could save computation time by avoiding massive contact detection between objects with different material properties, it may result in an inaccurate estimation of transmitted contact stresses on the pavement surface. To overcome this problem, a tire–pavement surface interaction model based on an implicit contact formulation that considers both tire and pavement characteristics and rolling conditions has been adopted [14]. The present tire loading boundary conditions satisfying different rolling conditions on the pavement surface were obtained from this model.

1.3. Literature review of asphalt mixture modeling

For the calculation of tire contact stresses, in most of researches, the asphalt mixture is assumed as homogeneous. This assumption is rational when we focus on the tire load distribution on the pavement surface as tire contact stresses can be realistically represented through the mesh-based methods in the continuum mechanics framework. However, when it comes to describe the internal asphalt mixture local responses, the homogenization assumption of asphalt mixture is insufficient as it cannot examine the mixture's mechanical performance from a microscopic level, consistently, at the particle level. Consequently, modeling a mixture structure while considering its different components and their respective properties explicitly is desired.

So far, FEM and DEM have become two major methodologies to model the microscopic structure of asphalt mixtures. To capture the heterogeneity and micro-structure of an asphalt mixture, FEM models were used to build an asphalt mixture with aggregates generated randomly by computer-aided algorithm [15] or reconstructed by X-ray computed tomography (CT) [16,17]. Using a FEM model with reconstructed aggregates, it was demonstrated that the angularity and irregular shape of coarse aggregates can be addressed in asphalt mixtures. However, these models are based on continuum mechanics theory, which still has difficulties in modeling contact status changes between various asphalt components as they come in and out of contact as well as sliding between different particles when in contact.

On the contrary, DEM is dedicated to the modeling of various complex and discontinuous assembly behaviors for interacting components. Thus, DEM offers a more promising way to model and characterize the micro-structure of an asphalt mixture at the particle level compared to FEM. A variety of studies have been conducted using DEM to investigate the micro-mechanical behavior of asphalt mixtures. To model the asphalt mastic, viscoelastic contact laws were widely used by researchers in recent years [18–20] to evaluate resilient modulus [21], permanent deformation mechanism [22] and compaction behavior of asphalt mixtures [23]. To depict realistic aggregate particles, many researches were conducted simulations on mixtures composed of irregular particle shapes, based on computer-aided algorithms [24–26], image scanning devices [27,28] and hybrid approaches of the two methods aforementioned [29]. However, in most of these studies, particle shapes are usually selected from limited templates or created randomly in the simulation. The particle morphology distribution in the real mixture assembly cannot be represented adequately in the numerical specimens due to the rich variability of actual particle shapes. Indeed, X-ray CT technique could be used to obtain the meso-structure of the whole asphalt sample, so that both particle morphology and size distributions would be better considered [30]. However, this method is physical specimen dependent, which cannot provide a fully numerical environment for asphalt mixture modeling. Besides, the model accuracy is also highly dependent on the image processing technique, which is usually time-consuming. Moreover, the CT device is usually expensive and lack of flexible mobility.

In the present study, a 3D micro-structural DEM model of an asphalt mixture developed in Ge et al. [31] is adopted. The model explicitly accounts for aggregate morphology distribution, particle size distribution and the activation of the viscoelastic contact model between aggregates, enabling a realistic depiction of heterogeneous asphalt mixture structure.

1.4. Coupling simulation of investigating asphalt mixture responses under tire loads

This paper aims to examine asphalt mixture responses under various tire rolling conditions at the particle level. There are several studies that have been carried out focusing on simplified wheel loading assumptions such as pulse loading, equivalent loading to predict the mechanical performance of asphalt pavements [32–35]. However, simplified loading conditions cannot reflect the non-uniform loading boundaries, and are not adequate to examine the pavement responses under real tire loading conditions [36]. Wollny et al. [37] proposed a consistent simulation chain based on FEM to examine the micro-structural asphalt model responses under realistic rolling tire loads. However, the simulation was conducted in the frame of FEM, which has limitations in describing contact status of individual particles.

On the other hand, several DEM models were built in 2D to investigate the asphalt layer responses under tire loads, including surface wear [38] and crack development [39]. However, the tire loading conditions used in current studies are usually uniform and simplified, which cannot reflect real non-uniform tire loads. Further, predicting the performance of asphalt mixtures based on 2D models might be unreliable due to the fact that they lack a full description of the heterogeneous structure of the asphalt mixture. Due to the computational costs involved in simulating tire load effects on asphalt mixtures using DEM in 3D, some DEM models simulate wheel tracking tests (WTTs) [22,25,40] to indirectly examine asphalt mixture responses under tire loads. Nevertheless, these simulations are compromised by size effects and simplified boundary conditions that come from WTTs, which inhibit accurate predictions of mixture responses.

Despite its promise in examining the mechanical properties of asphalt mixtures at the particle level, DEM is inadequate to accurately simulate deformable tire structures and capture realistic tire contact forces on pavement surfaces. Consequently, a multi-scale simulation incorporating FEM and DEM appears necessary to investigate non-uniform tire loads on asphalt mixtures at the particle level.

Herein, a multi-scale 3D FEM–DEM coupling simulation is presented to examine internal asphalt mixture responses micromechanically under rolling tire loads. Within this method, FEM is used to capture tire contact stresses on the pavement surface at a consistent level

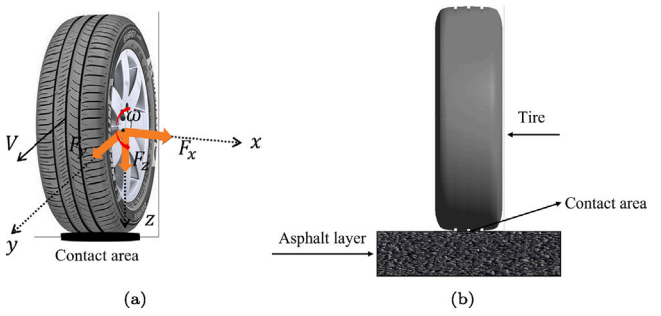

Fig. 1. (a) Tire driven forces during rolling (b) Tire–pavement model.

while DEM is dedicated to tracking particle movements and contact status changes in an asphalt mixture. We analyze statistically the micro-mechanical responses including particle movement characteristics, displacement and velocity distributions, contact forces, and individual particle displacement in an asphalt mixture under different tire rolling conditions. The current study proposes an innovative method for exploring tire–pavement interaction, which could help revealing degradation mechanisms of asphalt pavement surfaces under realistic tire rolling loads at the particle level.

2. Tire–pavement contact modeling

2.1. Modeling process and its calibration

A vehicle tire can withstand forces and torques from multiple axes, based on its rolling state. The vertical force results from vehicle weight, whereas the longitudinal force is generated when the tire is moving in a straight line during acceleration or braking. During cornering, the lateral force is generated with the changing tire direction. Fig. 1 illustrates the driven force status of a rolling tire and a classical tire–pavement model.

Fig. 2 presents the modeling process of the tire–pavement surface contact model. The tire geometry (185/65R15) was reconstructed by using laser scanning technique and the meshing process was performed by the open-source software Gmsh (https://gmsh.info/). In the tire–pavement interaction model, the tire structure was made up of a rigid rim and a deformable part representing rubber and air as a single component. For the sake of simplicity, we kept the longitudinal tire grooves while removing the transverse textures following the scanning results. Additionally, we replaced the rigid rim with a cylinder inheriting the same diameter. The deformable part was assumed as a homogeneous and elastic material with a modulus of 1.0 MPa and Poisson's ratio of 0.36 identified thanks to a force–displacement compression test, where the tire inflation pressure was 2.2 bar. To provide accurate and efficient solutions for tire contact stresses on the pavement surface, we built an asphalt layer with dimensions of 0.3 m × 0.3 m × 0.04 m and assumed that the pavement layer was homogeneous with an elastic modulus and Poisson's ratio of 13,000 MPa and 0.35, respectively. The simulation was conducted in the frame of FEM based on the implicit contact solving formulation through Contact Dynamics (CD) method [41,42]. LMGC90 (https://git-xen.lmgc.univ-montp2.fr/lmgc90/lmgc90_user/-/wikis/home), an implicit discrete element software dedicated to the modeling of large collections of interacting components (rigid or deformable) based on the CD method [43,44], has been adopted to build numerical models. More details about the tire modeling procedures can be found in a previous study [14].

We focused on the longitudinal tire behavior during free rolling, braking and acceleration. For a rolling tire without cornering, when a torque is applied to the tire, a longitudinal slip (k) occurs [45], defined as:

$$k = \begin{cases} -\dfrac{V_{y0} - r_w \cdot \omega}{V_{y0}} = -\dfrac{\omega_0 - \omega}{\omega_0}, a_v < 0 \\ \dfrac{r_w \cdot \omega - V_{y0}}{r_w \cdot \omega} = -\dfrac{\omega - \omega_0}{\omega}, a_v > 0 \end{cases} \quad (1)$$

where:

- V_{y0} [m/s] — rolling tire longitudinal velocity.
- r_w [m] — rolling tire radius.
- ω_0 [rad/s] — rolling tire angular velocity.
- k [-] — longitudinal tire slip.
- ω [rad/s] — braking/accelerating tire angular velocity.
- a_v [m/s^2] — vehicle acceleration.

For k different from zero, it corresponds to the acceleration ($k > 0$) or braking ($k < 0$) states, and the tire is subjected to longitudinal forces. The free rolling state is corresponding to $k = 0$, where only normal force is activated on the tire.

2.2. Tire contact stress distributions

The longitudinal forces associated with a tire under acceleration and braking are opposite but similar; therefore, the study only analyzed tire contact stresses under braking. Fig. 3 presents tire contact imprints on the pavement surface at free rolling and full braking (k=-1) conditions, where the normal tire load is 5 kN and the local friction coefficient between the tire and pavement surface is set to 0.8. Both contours demonstrate that the tire contact stress is not uniformly distributed, and the tire imprint is dissymmetric as it could be expected. The maximum contact stress area at full braking is concentrated along the y-axis due to the braking force action.

Fig. 4 displays that the tire induces contact stress components in both normal and tangential directions, which may affect pavement responses. Fig. 4(a) and 4(b) illustrate that the vertical contact stress at the two conditions presents similar non-uniform distribution across the whole contact area. The distribution of the vertical stress is symmetric along the y-axis, and the maximum stress values concentrate at the tire center ribs.

Regarding Fig. 4(c) and 4(d), the transverse stress distribution at free rolling and full braking conditions are very similar as no lateral force induced by corning acts on the tire. The lateral contact stress distributes symmetrically around the tire center and the stress values achieve maximum at the tire edge ribs.

At the two rolling conditions, the longitudinal contact stress is distributed symmetrically along the y-axis, with its peaks located at the center ribs of the tire, as shown in Fig. 4(e) and 4(f). Nevertheless, full braking perturbates greatly the longitudinal contact stress so as its distribution is largely dissymmetric with regards to the x-axis. As a consequence, longitudinal contact stress for the full braking condition is significantly higher than for the free rolling condition, which could accelerate pavement deterioration.

3. Asphalt mixture modeling

3.1. Complex modulus test set-up and modeling

The viscoelastic behavior of an asphalt mixture under cyclic loading can be assessed by the dynamic modulus $|E^*|$ and the phase angle Φ. To identify the mechanical properties of asphalt mixtures, complex modulus tests were conducted in a two-point bending (2PB) configuration according to the EN 12697-26:2012 specifications [46].

From a geometrical point of view, an asphalt mixture can be seen as a system of irregular particle tessellations, and particles interact with each other through mastic between them. In this study, we used

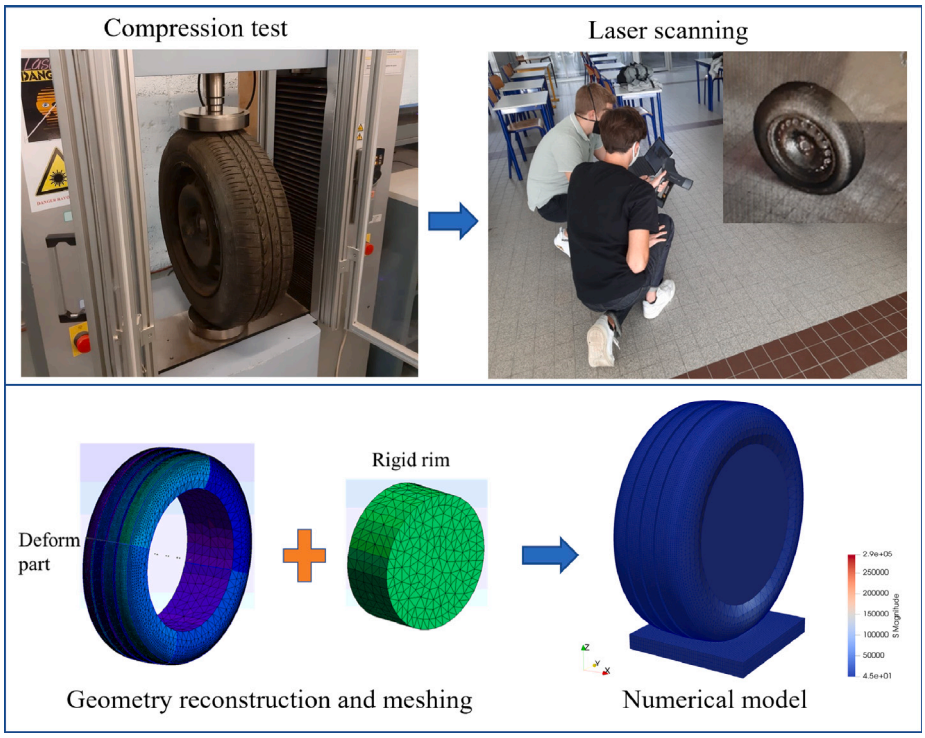

Fig. 2. Tire–pavement contact modeling process.

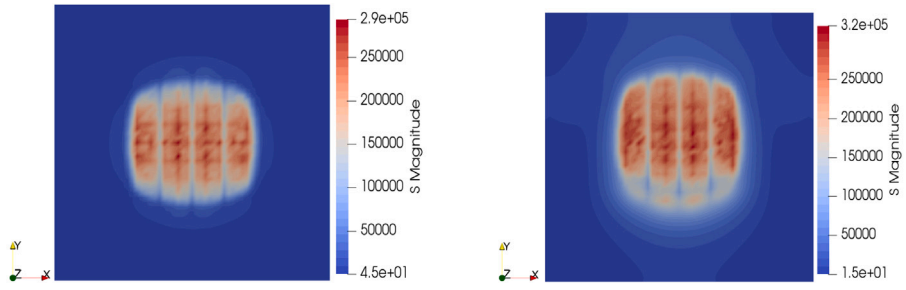

(a) Free rolling: Stress magnitude (b) Full braking: Stress magnitude

Fig. 3. Tire imprints at free rolling and full braking conditions.

the asphalt mixture model developed in a previous study [31] which incorporates particle morphology and particle size distribution into numerical simulations of asphalt mixtures.

Fig. 5 displays the test configuration and the numerical sample reconstructed in LMGC90 software. More details about the asphalt mixture modeling with irregular particles can be found in this previous study [31].

3.2. Calibration of the Burgers model

Asphalt mixture is a complex composite particular material showing a viscoelastic behavior, thus a viscoelastic contact model between particles based on the Burgers model is adopted in the simulation. This model comprises a Maxwell model put in series with a Kelvin–Voigt model, the stiffness and the viscosities for the Maxwell and the Kelvin–Voigt parts correspond to K_m, C_m, K_k, and C_k, respectively. More details about the numerical implementation of this contact model can be found in [20].

For a viscoelastic material under cyclic loading, it is possible to determine the complex compliance as following:

$$|D^*| = \sqrt{D'(\omega)^2 + D''(\omega)^2} \tag{2}$$

$$D'(\omega) = \frac{1}{K_m} + \frac{K_k}{{K_k}^2 + \omega^2 {C_k}^2} \tag{3}$$

$$D''(\omega) = \frac{1}{\omega C_m} + \frac{\omega C_k}{{K_k}^2 + \omega^2 {C_k}^2} \tag{4}$$

Where:

- K_m, C_m, K_k and C_k correspond to the Maxwell and Kelvin–Voigt stiffness and viscosities respectively.
- $|D^*|$ is the complex compliance, D' and D'' are the real and the imaginary parts of the complex compliance, and ω is the pulsation.

The master curve describing the loading time dependency of asphalt mixtures can be generated according to the time–temperature superposition principle. To build the corresponding master curve, a reference temperature T_{ref} was chosen, then the translation of all isotherm values were obtained from the temperature fit using the Williams–Landel–Ferry (WLF) transformation [47].

Fig. 6 shows the experimental and numerical results for the master curve for both the dynamic modulus and the phase angle. The numerical values from simulations are in good agreement with experimental values for $|E^*|$ and Φ for all the tested frequencies (from 3 up to 40 Hz)

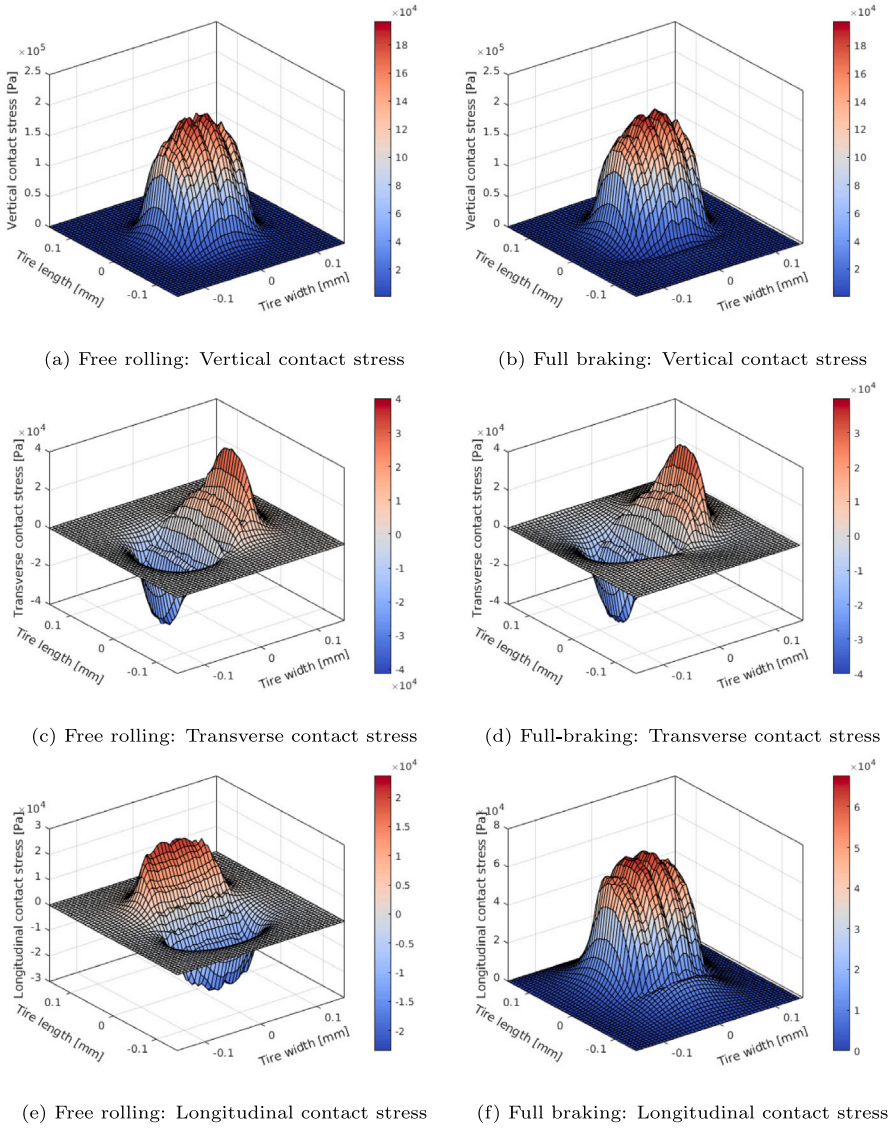

(a) Free rolling: Vertical contact stress

(b) Full braking: Vertical contact stress

(c) Free rolling: Transverse contact stress

(d) Full-braking: Transverse contact stress

(e) Free rolling: Longitudinal contact stress

(f) Full braking: Longitudinal contact stress

Fig. 4. Tire contact stress distributions at free rolling and full braking conditions.

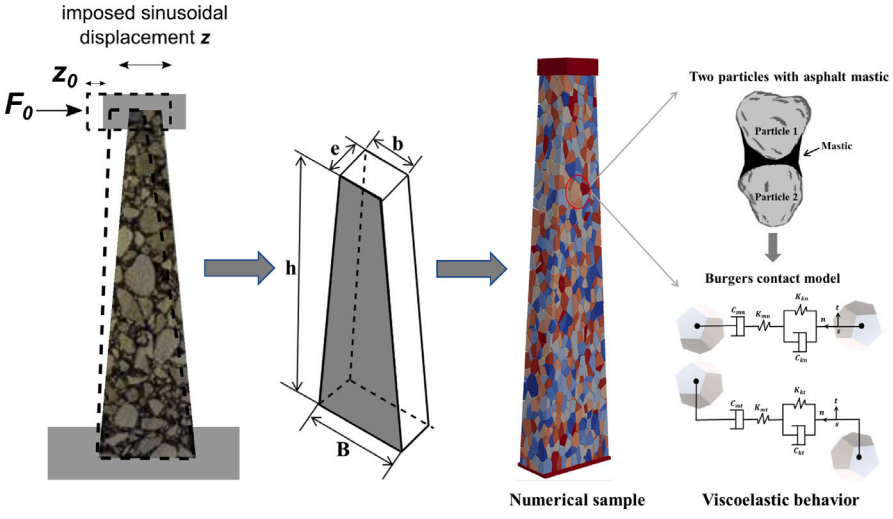

Fig. 5. 2PB test set-up and numerical modeling of test sample.

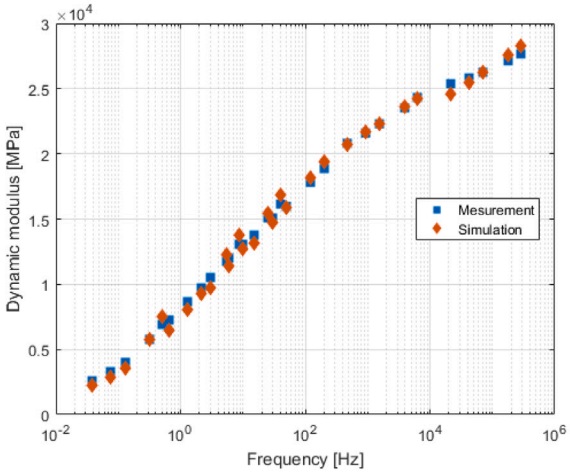

(a) Dynamic modulus

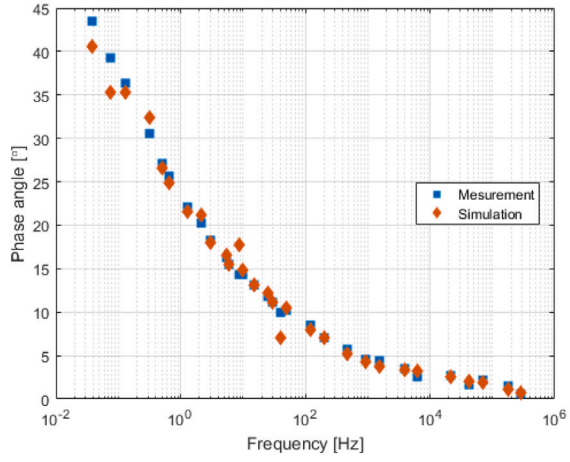

(b) Phase angle

Fig. 6. Experimental and numerical master curve at T_{ref} = 15 °C.

Table 1
Burgers model parameters used in numerical simulations.

T (°C)	K_m (Pa)	C_m (Pa s)	K_k (Pa)	C_k (Pa s)
15	9.48 × 10^7	1.02 × 10^7	1.70 × 10^8	1.79 × 10^6

and temperatures (between −10 and 30 °C), despite some fluctuations around the average values. The calibrated parameters determined by a mean square method for the Burgers contact model at T_{ref} = 15 °C were selected as input material properties in the later simulation, as listed in Table 1.

4. FEM-DEM coupling for the tire–pavement interaction

4.1. Coupling algorithm

The kernel of FEM–DEM coupling is based on the detection between tire contact forces and particles. This detection is conducted to determine which particle is in contact with the tire contact force ($\overrightarrow{F_n}$), where $\overrightarrow{F_n}$ is derived from the nodal force on the pavement surface from the FEM tire–pavement model, thus $\overrightarrow{F_n}$ is composed of three component F_{nx}, F_{ny}, F_{nz}. The coupling process is shown in Fig. 7.

At first, we focused on the contact area of the tire and pavement surface, so we extracted the tire imprint dimensions from the tire model. When the vertical tire force F_{nz} is lower than zero, the force position is deemed to be inside the tire–pavement surface contact area. After scanning all the force coordinates of the pavement surface, a square boundary area ($L_x \times L_y$) circumscribing all the contact force points could be obtained. Then, according to the square boundary dimensions, we created an asphalt mixture wearing layer with a thickness of 4 cm by using the calibrated asphalt mixture parameters. Afterward, the contact detection between the tire contact forces and asphalt mixture aggregates was performed during the simulation. Finally, the tire contact forces were applied to the particles on the asphalt mixture layer surface and the coupling simulation was conducted based on the time-iteration calculation frame. The general procedure is shown in algorithm Algorithm 1.

Algorithm 1 General procedure of the coupling algorithm.

1. Tire imprint determination
if F_{nz} <= 0 **then**
  1.1: Get coordinates of the contact force: F_{coorx}, F_{coory} and F_{coorz}
end if
2: Calculate the range of the contact force field: $L_x = max(F_{coorx}) - min(F_{coorx})$ and $L_y = max(F_{coory}) - min(F_{coory})$)
3: Asphalt mixture modeling according to the range.
loop
  4. Tire contact force detection on the surface layer
  if Tire contact force is inside the force field **then**
    4.1: Coarse detection
    4.2: Fine detection
  end if
  5. Tire contact force application on the asphalt mixture sample
  if The tire contact force is on a particle surface **then**
    5.1: Applying the force and moments to the particle
  end if
  6: Running next step simulation based on the time iteration algorithm

4.2. Tire contact force detection

For the tire contact force detection, we perform a detection at two levels: coarse detection and fine detection. As shown in Fig. 8, for a particle located on the asphalt layer surface, we first extracted its geometry information including polyhedron vertices. Then, we calculated the bounding box (minimal and maximal coordinates of vertices in x, y and z direction) of this particle and compared the tire contact force coordinates (F_{coor}) with the horizontal range of the bounding box, as shown in Fig. 8(a). If the tire contact force is outside the bounding box, it is judged that the contact force is outside all the particle surfaces. The tire contact force may also lie outside the particle surfaces while being in the bounding box, so we need to perform a further accurate detection, the fine detection. To perform fine detection, we extracted particle surfaces and compute a dot product to determine if the tire contact force is located on the particle surface. As shown in Fig. 8(b), a particle surface (ABC) is taken as an example. If the tire contact force point (P) is inside the triangle surface, the results of all the dot products ($\overrightarrow{AB} \cdot \overrightarrow{AP}$, $\overrightarrow{BC} \cdot \overrightarrow{BP}$, $\overrightarrow{CA} \cdot \overrightarrow{CP}$) must be higher than zero. The detection procedures are listed in the algorithm 2.

4.3. Tire contact force application

After the contact detection procedure, we need to apply the tire contact forces on particles located on the asphalt layer surface. For the contact force application, we applied external tire contact forces to the mass center of polyhedron particles. As shown in Fig. 9, as a tire contact force F_n has three components (F_{nx}, F_{ny} and F_{nz}), it can cause three components of moments (M_x, M_y and M_z) on the particle. By using the algorithm 3, the tire contact forces can be transmitted equally to the mass center as external forces and moments.

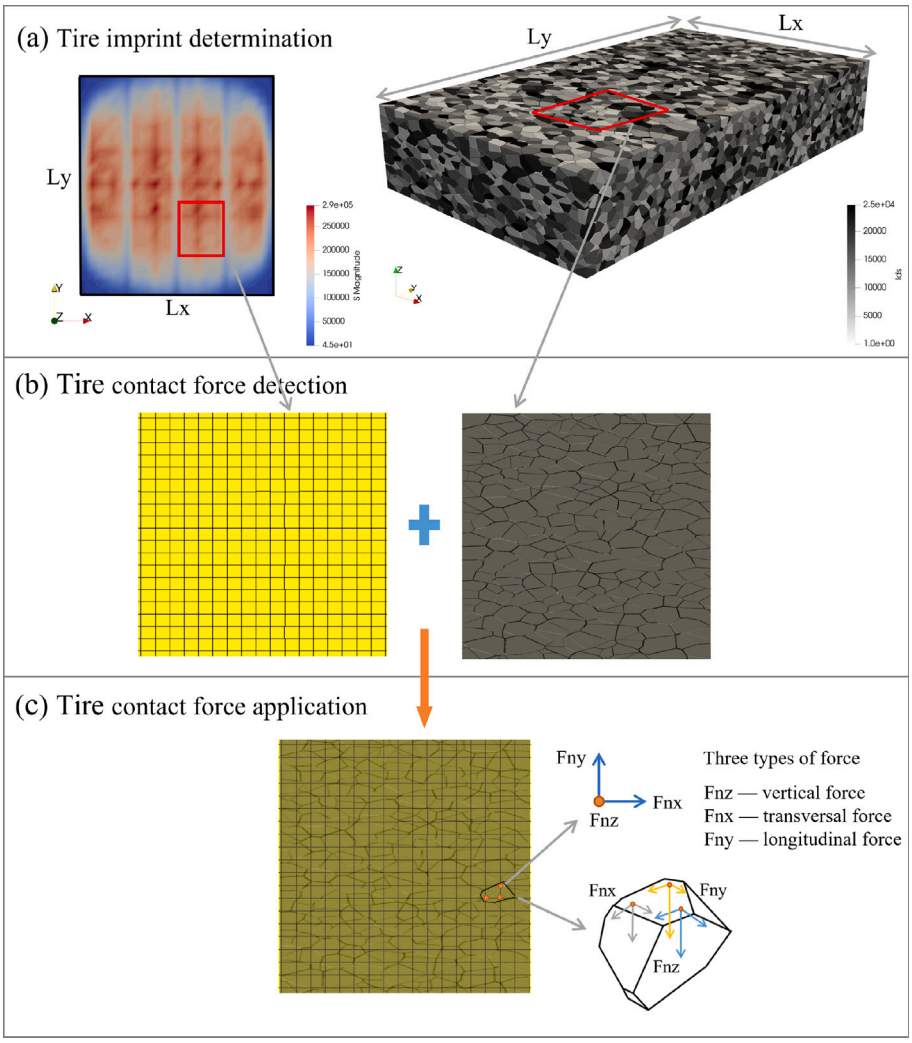

Fig. 7. Coupling simulation of FEM and DEM: (a) Tire imprint determination (b) Contact force detection (c) Contact force application.

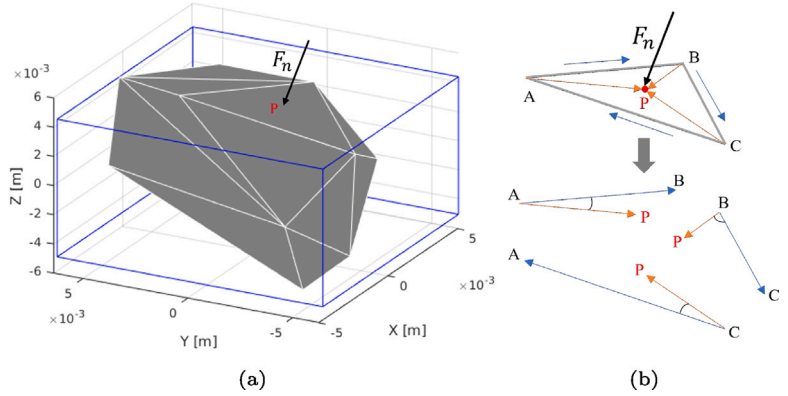

Fig. 8. (a) Coarse detection: Bounding box (b) Fine detection: Point in polyhedron.

5. Results and discussion

In this section, we investigate the mechanical response of the asphalt mixture layer under varying tire rolling conditions including rolling velocity and rolling status. All the simulation were conducted in LMGC90 at T_{ref} = 15 °C, which is a referenced value in French pavement design [46]. For the entire simulation, the bottom particles in the asphalt layer model are fixed by a rigid wall, which provides a bottom boundary condition. Besides, thanks to the symmetric distribution of tire contact stresses, a symmetric simulation strategy was adopted

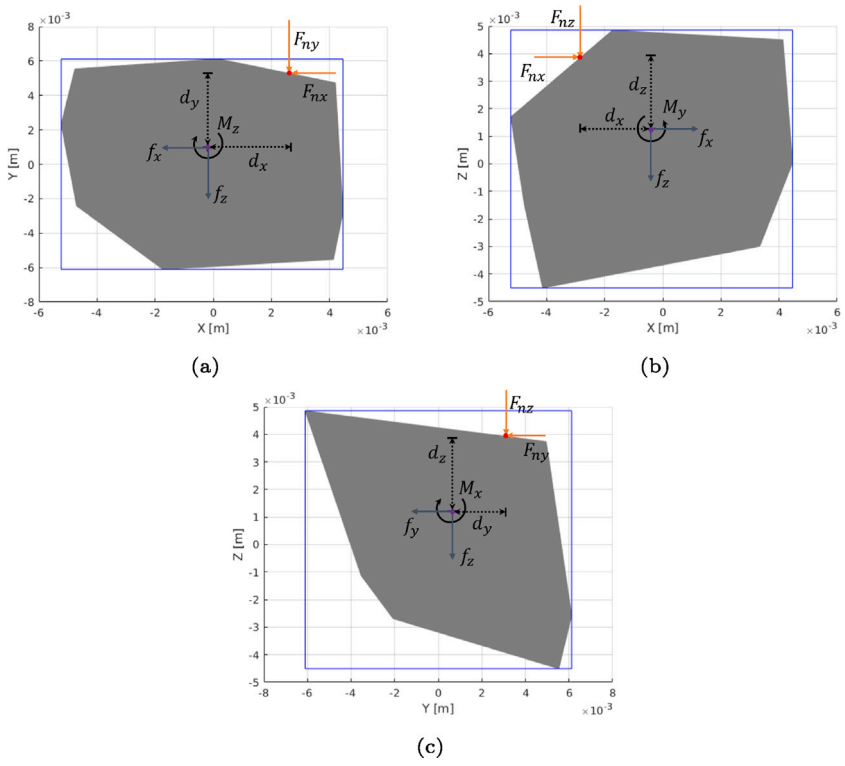

Fig. 9. (a) Plane-XY (b) Plane-XZ (c) Plane-YZ.

Algorithm 2 Tire contact force detection on the particle.

1. Coarse detection
if $min(Xvertex) <= F_{coorx} <= max(Xvertex)$, *and* $min(Yvertex) <= F_{coory} <= max(Yvertex)$ **then**
  Particle is on the bounding box surface of the particle
  2. Fine detection
  if $\overrightarrow{AB} \cdot \overrightarrow{AP} >= 0$, and $\overrightarrow{BC} \cdot \overrightarrow{BP} >= 0$, and $\overrightarrow{CA} \cdot \overrightarrow{CP} >= 0$ **then**
    Force is on the particle surface
  else
    Force is outside the particle surface
  end if
else
  Force is outside the particle surface
end if

Algorithm 3 Tire contact force application to the particle.

1. External particle force f calculation
if Tire contact force point is on the particle surface **then**
  $f_x = F_{nx}$
  $f_y = F_{ny}$
  $f_z = F_{nz}$
  2. External particle moment M calculation
  $M_x = F_{ny} * dz + F_{nz} * dy$
  $M_y = F_{nx} * dz + F_nz * dx$
  $M_z = F_{nx} * dy + F_{ny} * dx$
end if

to reduce the computation cost. The simulation used only half of the layer model along the y-axis, whereas the x-direction of particles on the center surface was fixed simultaneously to provide a lateral boundary condition. The time step was set to 5×10^{-5} s for all simulations to ensure the numerical stability. The CPU time was 3.2×10^{-3} s per particle and per time step on a Dell computer of speed 3.9 GHz.

5.1. Effects of tire rolling velocity

5.1.1. Bottom boundary force

Three tire rolling velocities (10, 20, and 30 m/s) were applied to the coupling model at the free rolling condition to investigate the effect of tire rolling velocity on mixture layer responses. Fig. 10(a) gives evolution results for the bottom boundary force at tire velocity of 30 m/s along the time. All the force values first increase until they reach their peak values, and then they all decrease gradually down to zero. Besides, the vertical force is dominating the mixture layer, while tangential forces are relatively lower.

Fig. 10(b) compares F_z (vertical component of the boundary force) at different tire velocities. A similar evolution trend can be observed for F_z under different tire loading velocities, with a similar peak value achieved in the middle of the loading time for each tire velocity. It seems that the velocity has no significant influence on the Fz peak value as it could have been expected.

5.1.2. Contact force network evolution

In particle-based methods, contact force networks reflect external loads transmitted through granular materials. Coexisting strong and weak contacts form a contact network, which is made up of the corresponding strong contact forces, i.e. forces above the mean normal value ($f_n > \langle f_n \rangle$), and weak contact forces ($f_n < \langle f_n \rangle$) [48].

Fig. 11 shows the strong and weak force distribution during the rolling process at a tire velocity of 30 m/s. In response to moving tire load, strong (red) and weak (blue) forces evolved. At the initial stage of rolling (T = 0.0015 s), the contact force network is considerably loose because only a little range of tire load activates on the layer surface.

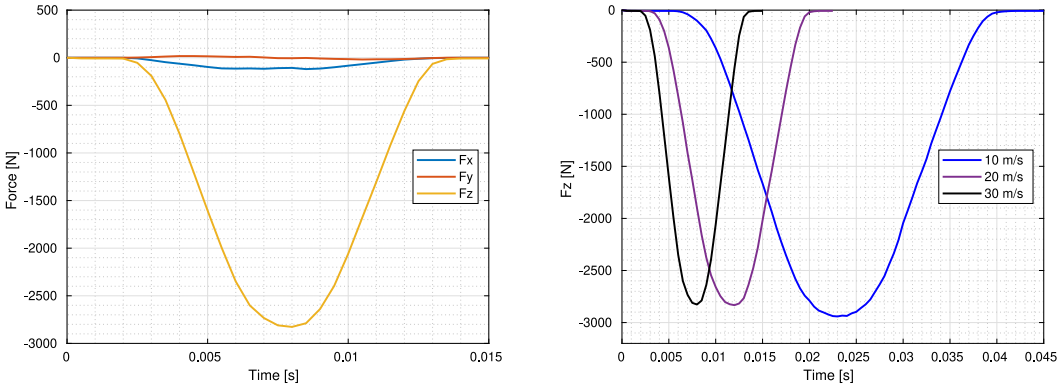

(a) Boundary force at free rolling (30 m/s) (b) Comparison for F_z at different rolling speeds

Fig. 10. Bottom boundary force characteristics.

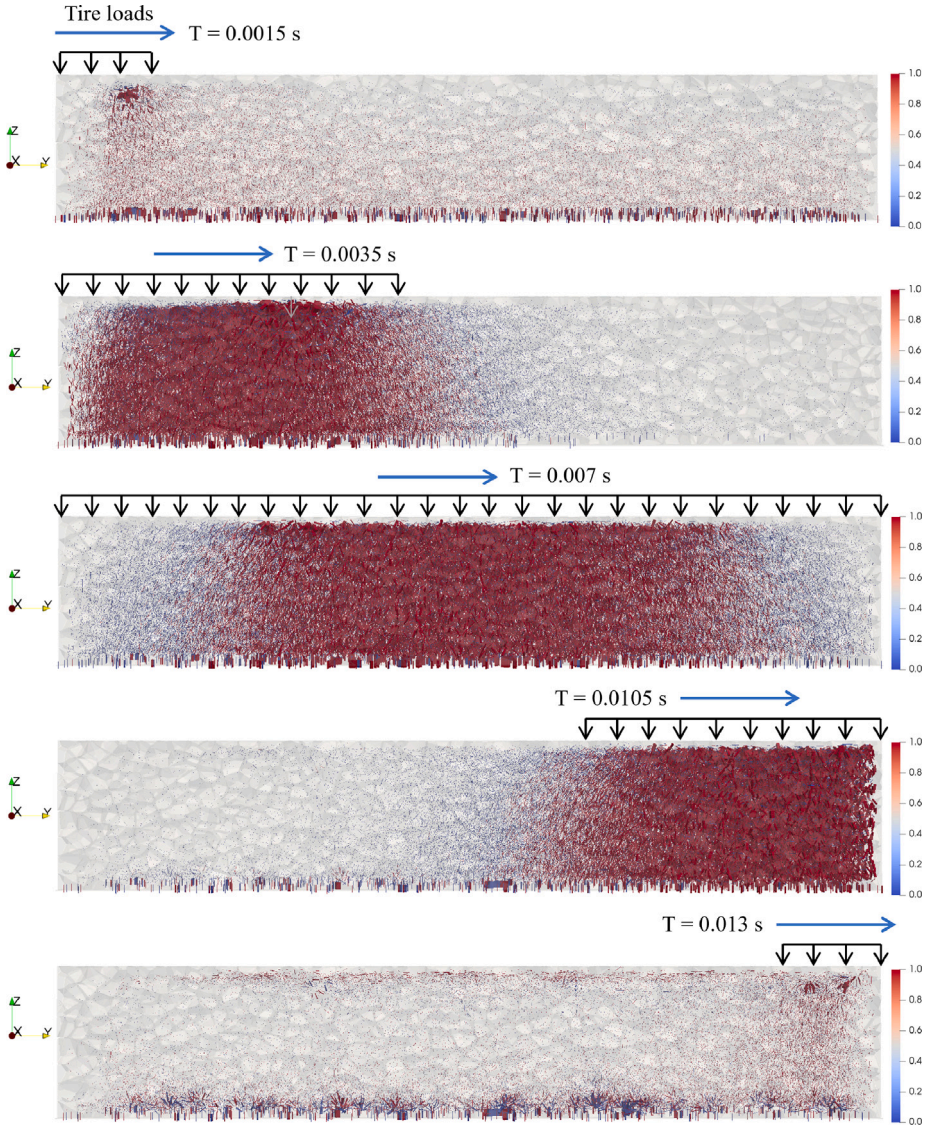

Fig. 11. Contact force network evolution (strong force = 1.0 and weak force = 0.0) at rolling velocity of 30 m/s. (For interpretation of the references to color in this figure legend, the reader is referred to the web version of this article.)

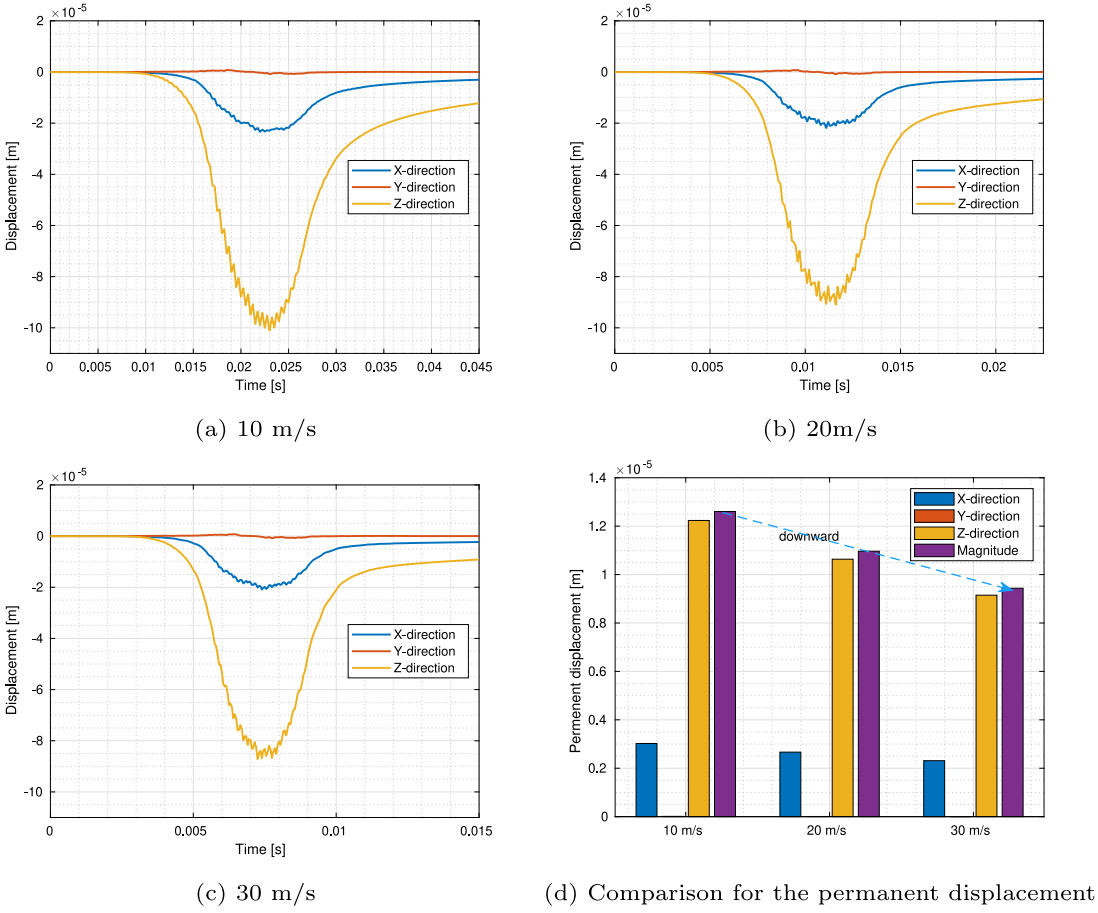

(a) 10 m/s (b) 20m/s

(c) 30 m/s (d) Comparison for the permanent displacement

Fig. 12. Particle displacement for different tire rolling speeds.

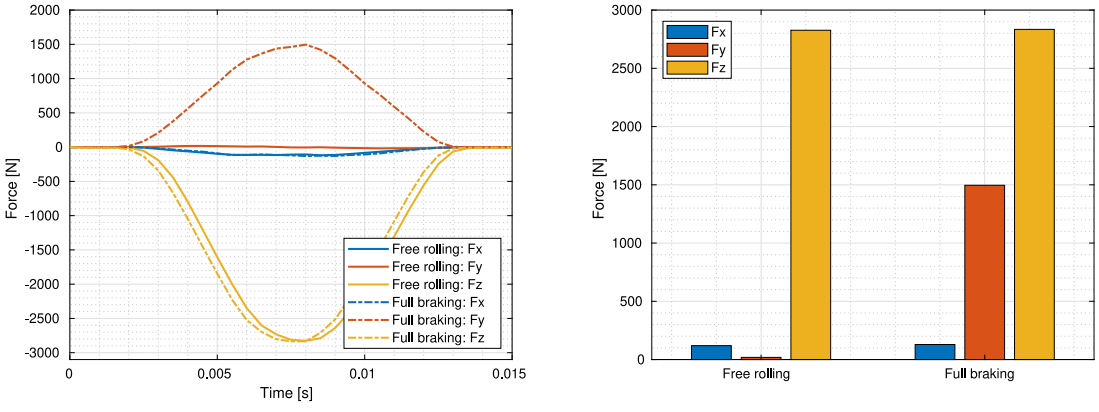

(a) Boundary force F comparison (b) Peak force value comparison

Fig. 13. Bottom boundary force characteristics for different rolling status.

When the tire load is fully distributed on the mixture layer (T = 0.007 s), the strong contact force network reaches its maximum distribution range. After that, as the tire load passes from the layer surface, the strength of force networks starts to diminish. A relatively equal balance of force states is finally achieved (after $T = 0.013$ s) when the tire load fully passes the layer surface. An analysis of the evolution of the contact networks shows how the tire is moving on the asphalt layer surface, demonstrating the effectiveness of the coupling algorithm.

5.1.3. Particle movement characteristics

Further, we investigate the movement of individual particles during the rolling process under different tire velocities. Fig. 12 depicts the movement evolution of one particle located on the center of the surface layer under various tire rolling speeds. Throughout the loading duration, particle displacement increases, and it reaches its peak value halfway through the loading time. It then decreases gradually until it reaches its residual value. It can be found that particle displacement

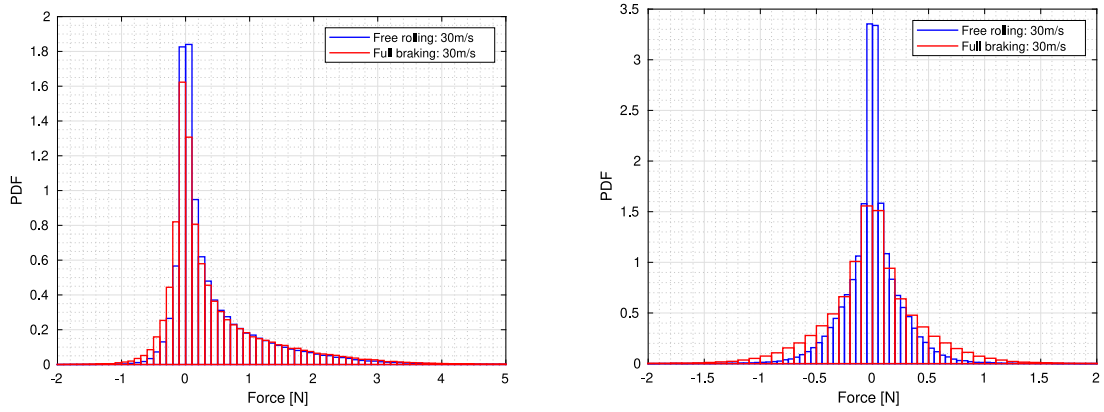

(a) Normal contact force (b) Tangential contact force

Fig. 14. Particle contact force distribution at different tire rolling status.

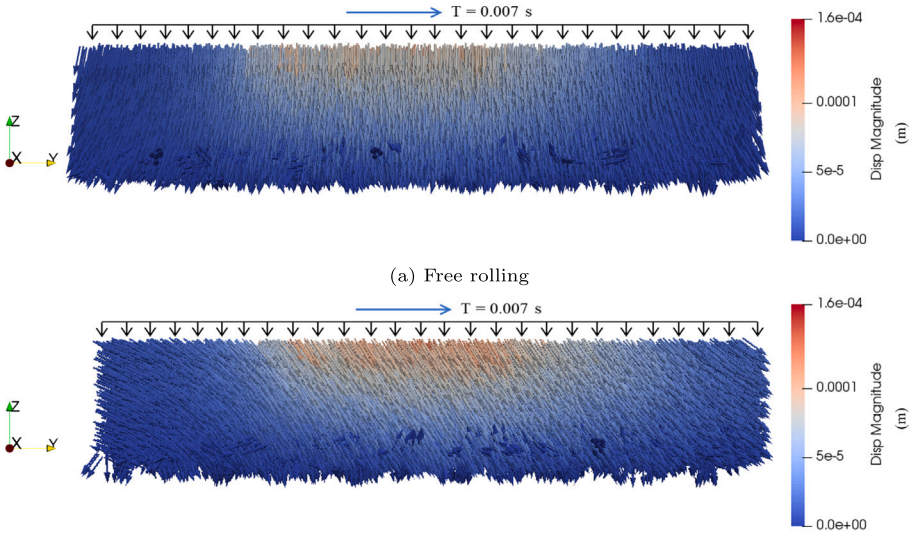

(a) Free rolling

(b) Full braking

Fig. 15. Particle displacement distribution at 30 m/s for different rolling status (T = 0.007 s)

is mainly caused by vertical particle movement due to strong vertical tire contact forces. Fig. 12(a), 12(b) and 12(c) illustrate that the value of particle displacement cannot return to zero after a tire load passes, which indicates that the tire load causes residual strains due to the viscous flow occurring within the asphalt mixture. The accumulation of the particle displacement after multiple tire load cycles could finally lead to macroscopic non-recoverable plastic deformation such as rutting. Tire load-induced plastic deformation is referred to as permanent displacement here. Fig. 12(d) illustrates the permanent displacement of the particle at different tire speeds. According to the results, low tire speed induces high permanent displacement for particles, which is in agreement with the measurement observations that low tire speed causes severe rutting.

5.2. Effects of tire rolling status

5.2.1. Bottom boundary force

Fig. 13 shows the boundary force comparison for free rolling and full brake conditions. Compared to the free rolling condition, the boundary force has a significant component along the longitudinal axis (y-axis) at full braking, which could result in particle disturbances in the mixture.

5.2.2. Particle contact force distribution

Furthermore, the particle contact force distribution under two loading conditions was analyzed. The time points corresponding to the peak boundary values were selected as critical times to study the particle contact force distribution.

There are two types of forces acting at the particle contact plane: the tangential force that induces shearing, and the normal force lying perpendicular to the contact plane. The combination of both forces can result in particle contact breakage and particles moving, resulting in macro-cracks forming and propagating within the mix. A comparison of normal contact force distributions for particles at free rolling and full braking conditions is shown in Fig. 14(a). As a result of the similar vertical contact stresses at two loading conditions, normal force value distributions are mostly asymmetric along the y-axis (x=0). The main reason being that particles under both loading conditions generally suffer from a compression state.

As shown in Fig. 14(b), the tangential contact force values vary depending on the loading conditions. For both free rolling and full braking conditions, the tangential contact force values follow approximately a normal distribution with zero at the center. Under the full braking condition, the magnitude range of tangential force values is greater than that under the free rolling condition, which indicates that

(a) Translation velocity-free rolling

(b) Angular velocity-free rolling

(c) Translation velocity-full braking

(d) Angular velocity-full braking

Fig. 16. Average particle velocities for different tire rolling status.

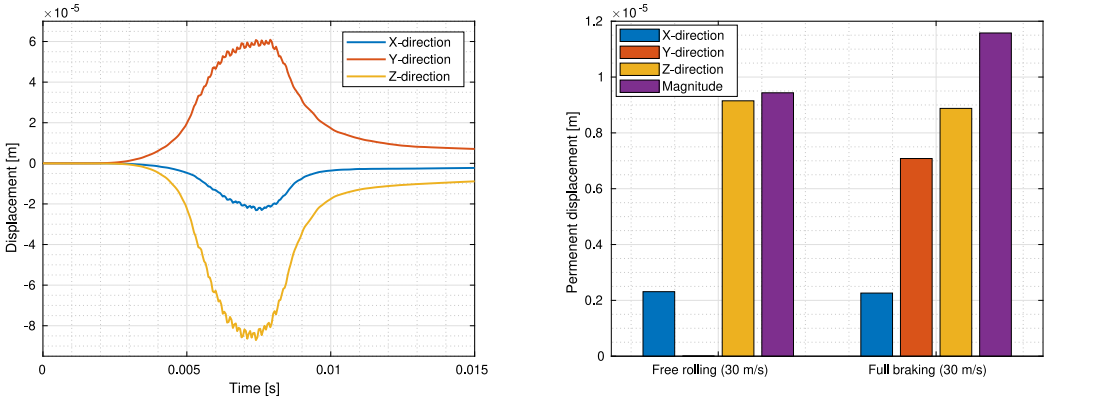

(a) Full braking (30m/s)

(b) Comparison for the permanent displacement

Fig. 17. Particle displacement for different tire rolling status.

full braking induces a stronger shear effect between particles, which may lead to earlier initiation of damage within the mixture.

5.2.3. *Particle displacement distribution*

Fig. 15 presents the particle displacement distribution for both loading conditions. The particle displacement distribution under free rolling is shown in Fig. 15(a). The arrows in the figure indicate particle movement direction, and their colors indicate particle displacement magnitude. The particle displacements are not distributed uniformly in the mixture, with particles near the center displacing more than those in other regions, which is consistent with the concentration of stresses under free rolling. The direction of the arrow is primarily vertical because the vertical tire contact stress dominates. Due to the existence of longitudinal and lateral tire contact stresses, particles lying on both sides have a significant horizontal component of particle displacement.

Fig. 15(b) shows the particle displacement distribution under the full braking condition. There is a visible concentration of peak displacements on one side of the model along the longitudinal axis. As a result

of the significant longitudinal contact stress, particle displacement arrows also have an obvious longitudinal component.

5.2.4. Average particle velocity

Fig. 16 gives the evolution of average particle velocity including translation velocity and angular velocity for two loading conditions. The alignment of the translation velocity at full braking (Fig. 16(c)) exhibits a higher component of velocity along the *y*-axis than that at free rolling (Fig. 16(a)), which indicates that particles tend to move along the *y*-axis during full braking. The comparison of the angular velocity characteristics at two loading conditions shows the particles tend to have a noticeable rotation along the *x*-axis at full braking, as indicated by Fig. 16(b) and 16(d).

5.2.5. Particle movement characteristics

Additionally, the displacement of a single particle is investigated. Fig. 17 shows the displacement evolution of one particle located on the layer surface center under both loading conditions. It can be found that the full braking condition causes an obvious longitudinal displacement component (Fig. 17(a)) during the tire rolling process and a permanent displacement component (Fig. 17(b)) along the *y*-axis after the tire rolling.

Tire rolling conditions including tire speed and rolling status are crucial in examining the mixture responses of asphalt surface layers. It is inevitable that tangential contact stresses are caused by the tire, particularly during braking or acceleration, which are crucial factors in asphalt mixture performance. The assumption of uniform contact stress is insufficient for predicting surface failures of asphalt mixtures, and it could lead to a misinterpretation of pavement degradation mechanisms under tire loads. The FEM–DEM coupling analysis described above offers insights into pavement surface design at the particle level by analyzing asphalt mixture responses under rolling tire loads using both continuum and discrete mechanics methods.

6. Conclusion

The present study developed a FEM–DEM coupling frame to study asphalt mixture responses at the particle level under real rolling tire loads. The main conclusions are drawn as follows:

In order to provide realistic tire loads, a numerical tire model based on FEM has been developed, and tire contact stress distributions under free rolling and full braking have been compared. An asphalt mixture layer comprised of irregular aggregate particles was then constructed via DEM, and the parameters of the viscoelastic contact model were identified through the complex modulus test. Finally, the tire contact forces were derived from the FEM tire model and applied to the DEM model of asphalt mixture as boundary conditions to examine internal mixture behaviors at real tire loads.

A FEM–DEM coupling algorithm was developed for the tire–pavement surface interaction process. Three procedures including tire imprint determination, tire contact force detection, and tire contact force application were performed continuously. The coupling simulation was performed to examine the response of the asphalt mixture layer to rolling tire loads based on the time step iteration.

As the tire rolls on the asphalt layer surface, the particle contact force network evolves in a consistent way with the loading process, demonstrating the effectiveness of coupling simulations. In the study of the effect of tire velocity on mixture responses, it was found that low tire velocity results in a large permanent particle displacement, which might eventually result in a large non-recoverable permanent mixture deformation.

The effect of tire rolling state on asphalt mixture behavior has been demonstrated in a study showing particle contact force at full braking is higher than that at free rolling. At the contact plane, full braking causes a great amount of shear, which may lead to early damage initiation. According to the particle displacement distribution, particles tend to flow and rotate along the longitudinal direction under full braking, resulting in structural disturbance. Moreover, due to tire boundary forces along the longitudinal direction under full braking, particles tend to have a large displacement component along the direction, which could result in severe permanent deformation.

The coupling method incorporating both FEM and DEM provides a promising way for analyzing asphalt mixture responses micro-mechanically under realistic rolling tire loads and may give insight into the surface design of asphalt pavements. The next step consists to proceed further with particle-scale damage analysis, and bridging it with macroscopic pavement performance predictions.

CRediT authorship contribution statement

Haitao Ge: Conceptualization, Software, Investigation, Writing – original draft, Visualization. **Juan Carlos Quezada:** Conceptualization, Software, Writing – review & editing. **Vincent Le Houerou:** Writing – review & editing. **Cyrille Chazallon:** Writing – review & editing, Funding acquisition, Supervision.

Declaration of competing interest

The authors declare that they have no known competing financial interests or personal relationships that could have appeared to influence the work reported in this paper.

Data availability

Data will be made available on request.

Acknowledgments

The work presented in this paper was financially supported by the French National Research Agency (SolDuGri project ANR-14-CE22-0001). The first author gratefully acknowledges financial support from China Scholarship Council (No. 201806560055).

References

[1] A. Gonzalez, M. Cubrinovski, B. Pidwerbesky, D. Alabaster, Full-scale experiment on foam bitumen pavements in an accelerated testing facility, Transp. Res. Rec. 2094 (1) (2009) 21–29.
[2] S. Chun, K. Kim, J. Greene, B. Choubane, Evaluation of top-down cracking potential for asphalt pavements with 4.75 mm nominal maximum aggregate size mixture layer using full-scale field tests and finite element analysis, Road Mater. Pavement Des. 19 (5) (2018) 1089–1101.
[3] M. Nguyen, P. Hornych, X. Le, M. Dauvergne, L. Lumière, C. Chazallon, M. Sahli, S. Mouhoubi, D. Doligez, E. Godard, Development of a rational design procedure based on fatigue characterisation and environmental evaluations of asphalt pavement reinforced with glass fibre grid, Road Mater. Pavement Des. 22 (sup1) (2021) S672–S689.
[4] W. Wang, K. Zhao, J. Li, R. Luo, L. Wang, Characterization of dynamic response of asphalt pavement in dry and saturated conditions using the full-scale accelerated loading test, Constr. Build. Mater. 312 (2021) 125355.
[5] M. De Beer, C. Fisher, Stress-in-motion (SIM) system for capturing tri-axial tyre–road interaction in the contact patch, Measurement 46 (7) (2013) 2155–2173.
[6] E.Y. Manyo, P. Reynaud, B. Picoux, R. Tautou, D. Nelias, F. Allou, C. Petit, Towards fast modelling of the tire-pavement contact, Eur. J. Environ. Civ. Eng. 25 (13) (2021) 2396–2412.
[7] Y. Oubahdou, E. Wallace, P. Reynaud, B. Picoux, J. Dopeux, C. Petit, D. Nélias, Effect of the tire–pavement contact at the surface layer when the tire is tilted in bend, Constr. Build. Mater. 305 (2021) 124765.
[8] N. Korunović, M. Trajanović, M. Stojković, Finite element model for steady-state rolling tire analysis, J. Serbian Soc. Comput. Mech. 1 (1) (2007) 63–79.
[9] H. Wang, I.L. Al-Qadi, I. Stanciulescu, Simulation of tyre–pavement interaction for predicting contact stresses at static and various rolling conditions, Int. J. Pavement Eng. 13 (4) (2012) 310–321.
[10] I. Wollny, M. Kaliske, Numerical simulation of pavement structures with inelastic material behaviour under rolling tyres based on an arbitrary Lagrangian Eulerian (ALE) formulation, Road Mater. Pavement Des. 14 (1) (2013) 71–89.

[11] I. Wollny, R. Behnke, K. Villaret, M. Kaliske, Numerical modelling of tyre–pavement interaction phenomena: coupled structural investigations, Road Mater. Pavement Des. 17 (3) (2016) 563–578.
[12] M. Guo, X. Zhou, Tire-pavement contact stress characteristics and critical slip ratio at multiple working conditions, Adv. Mater. Sci. Eng. 2019 (2019).
[13] M. Guo, X. Li, M. Ran, X. Zhou, Y. Yan, Analysis of contact stresses and rolling resistance of truck-bus tyres under different working conditions, Sustainability 12 (24) (2020) 10603.
[14] H. Ge, V. Quezada, C. Chazallon, Multiscale analysis of tire and asphalt pavement interaction via coupling FEM–DEM simulation, Eng. Struct. 256 (2022) 113925.
[15] J. Chen, H. Wang, L. Li, Virtual testing of asphalt mixture with two-dimensional and three-dimensional random aggregate structures, Int. J. Pavement Eng. 18 (9) (2017) 824–836.
[16] P. Liu, J. Hu, D. Wang, M. Oeser, S. Alber, W. Ressel, G.C. Falla, Modelling and evaluation of aggregate morphology on asphalt compression behavior, Constr. Build. Mater. 133 (2017) 196–208.
[17] C. Jin, F. Zou, X. Yang, K. Liu, 3-D virtual design and microstructural modeling of asphalt mixture based on a digital aggregate library, Comput. Struct. 242 (2021) 106378.
[18] Y. Liu, Q. Dai, Z. You, Viscoelastic model for discrete element simulation of asphalt mixtures, J. Eng. Mech. 135 (4) (2009) 324–333.
[19] G. Dondi, V. Vignali, M. Pettinari, F. Mazzotta, A. Simone, C. Sangiorgi, Modeling the DSR complex shear modulus of asphalt binder using 3D discrete element approach, Constr. Build. Mater. 54 (2014) 236–246.
[20] J.C. Quezada, C. Chazallon, Complex modulus modeling of asphalt concrete mixes using the non-smooth contact dynamics method, Comput. Geotech. 117 (2020) 103255.
[21] L. Gaillard, J.C. Quezada, C. Chazallon, P. Hornych, Resilient modulus prediction of RAP using the contact dynamics method, Transp. Geotech. 24 (2020) 100371.
[22] H. Wang, Z. Zhou, W. Huang, X. Dong, Investigation of asphalt mixture permanent deformation based on three-dimensional discrete element method, Constr. Build. Mater. 272 (2021) 121808.
[23] E. Olsson, D. Jelagin, M.N. Partl, New discrete element framework for modelling asphalt compaction, Road Mater. Pavement Des. 20 (sup2) (2019) S604–S616.
[24] D. Zhang, X. Huang, Y. Zhao, Algorithms for generating three-dimensional aggregates and asphalt mixture samples by the discrete-element method, J. Comput. Civ. Eng. 27 (2) (2013) 111–117.
[25] B. Xue, J. Xu, J. Pei, J. Zhang, R. Li, Investigation on the micromechanical response of asphalt mixture during permanent deformation based on 3D virtual wheel tracking test, Constr. Build. Mater. 267 (2021) 121031.
[26] J.C. Quezada, C. Chazallon, Discrete element modelling of hot mix asphalt complex modulus using realistic aggregate shapes, Road Mater. Pavement Des. 23 (sup1) (2022) 178–195.
[27] J. Hu, T. Ma, K. Ma, DEM-CFD simulation on clogging and degradation of air voids in double-layer porous asphalt pavement under rainfall, J. Hydrol. 595 (2021) 126028.
[28] A. Garcia, S. Michot-Roberto, S. Dopazo-Hilario, A. Chiarelli, A. Dawson, Creation of realistic virtual aggregate avatars, Powder Technol. (2020).
[29] J. Chen, H. Wang, H. Dan, Y. Xie, Random modeling of three-dimensional heterogeneous microstructure of asphalt concrete for mechanical analysis, J. Eng. Mech. 144 (9) (2018) 04018083.
[30] Z. You, S. Adhikari, M. Emin Kutay, Dynamic modulus simulation of the asphalt concrete using the X-ray computed tomography images, Mater. Struct. 42 (5) (2009) 617–630.
[31] H. Ge, J.C. Quezada, V. Le Houerou, C. Chazallon, Three-dimensional simulation of asphalt mixture incorporating aggregate size and morphology distribution based on contact dynamics method, Constr. Build. Mater. 302 (2021) 124124.
[32] D. Bodin, J.R. Grenfell, A.C. Collop, Comparison of small and large scale wheel tracking devices, Road Mater. Pavement Des. 10 (sup1) (2009) 295–325.
[33] E.Y. Chen, E. Pan, T.S. Norfolk, Q. Wang, Surface loading of a multilayered viscoelastic pavement: moving dynamic load, Road Mater. Pavement Des. 12 (4) (2011) 849–874.
[34] R.K. Abu Al-Rub, M.K. Darabi, C.-W. Huang, E.A. Masad, D.N. Little, Comparing finite element and constitutive modelling techniques for predicting rutting of asphalt pavements, Int. J. Pavement Eng. 13 (4) (2012) 322–338.
[35] C. Du, P. Liu, Y. Sun, J. Chen, Q. Liu, M. Oeser, Characterizing asphalt mixtures with random aggregate gradations based on the three-dimensional locally homogeneous model, Comput.-Aided Civ. Infrastruct. Eng. (2021).
[36] X. Jiang, C. Zeng, X. Gao, Z. Liu, Y. Qiu, 3D FEM analysis of flexible base asphalt pavement structure under non-uniform tyre contact pressure, Int. J. Pavement Eng. 20 (9) (2019) 999–1011.
[37] I. Wollny, F. Hartung, M. Kaliske, P. Liu, M. Oeser, D. Wang, G. Canon Falla, S. Leischner, F. Wellner, Coupling of microstructural and macrostructural computational approaches for asphalt pavements under rolling tire load, Comput.-Aided Civ. Infrastruct. Eng. 35 (11) (2020) 1178–1193.
[38] H. Dan, L. Gao, H. Wang, J. Tang, Discrete-element modeling of mean texture depth and wearing behavior of asphalt mixture, J. Mater. Civ. Eng. 34 (4) (2022) 04022027.
[39] S. Xie, J. Yi, H. Wang, S.-H. Yang, M. Xu, D. Feng, Mechanical response analysis of transverse crack treatment of asphalt pavement based on DEM, Int. J. Pavement Eng. 23 (7) (2022) 2206–2226.
[40] T. Ma, D. Zhang, Y. Zhang, S. Wang, X. Huang, Simulation of wheel tracking test for asphalt mixture using discrete element modelling, Road Mater. Pavement Des. 19 (2) (2018) 367–384.
[41] J.J. Moreau, Unilateral contact and dry friction in finite freedom dynamics, in: Nonsmooth Mechanics and Applications, Springer, 1988, pp. 1–82.
[42] M. Jean, The non-smooth contact dynamics method, Comput. Methods Appl. Mech. Engrg. 177 (3–4) (1999) 235–257.
[43] F. Dubois, V. Acary, M. Jean, The contact dynamics method: A nonsmooth story, C. R. Méc. 346 (3) (2018) 247–262.
[44] F. Radjai, V. Richefeu, Contact dynamics as a nonsmooth discrete element method, Mech. Mater. 41 (6) (2009) 715–728.
[45] H. Pacejka, Tire and Vehicle Dynamicss, second ed., Butterworth-Heinemann, Oxford, UK, 2005, 2006.
[46] EN12697-26, Bituminous Mixtures–Test Methods for Hot Mix Asphalt–Part 26: Stiffness, afnor edition, 2012.
[47] M.L. Williams, R.F. Landel, J.D. Ferry, The temperature dependence of relaxation mechanisms in amorphous polymers and other glass-forming liquids, J. Am. Chem. Soc. 77 (14) (1955) 3701–3707.
[48] E. Azéma, F. Radjai, G. Saussine, Quasistatic rheology, force transmission and fabric properties of a packing of irregular polyhedral particles, Mech. Mater. 41 (6) (2009) 729–741.